European Polymer Journal 120 (2019) 109251

Contents lists available at ScienceDirect

European Polymer Journal

journal homepage: www.elsevier.com/locate/europolj

Investigating the effects of bulky allylic substituents on the regioregularity and thermodynamics of ROMP on cyclopentene

Gina A. Guillory, Justin G. Kennemur*

Department of Chemistry and Biochemistry, Florida State University, Tallahassee, FL 32303, United States

ARTICLE INFO

Keywords:
ROMP
Thermodynamics
Polypentenamer
Regioregularity

ABSTRACT

The interplay between equilibrium ROMP thermodynamics and the regioregular insertion of allylic trialkylsiloxy-substituted cyclopentenes during propagation with Hoveyda-Grubbs 2nd generation catalyst at varying temperatures is investigated. In general, bulkier substituents reduce monomer conversion and increase regioregular insertion. However, polymerization entropy (ΔS_p) also appears to play an important role on ROMP thermodynamics when compared to ring strain (ΔH_p) which is typically the parameter of focus for the efficacy of low-strain monomer conversion. This analysis has allowed for the determination of a "Goldilocks" monomer (i.e. one that provides the best compromise of monomer conversion (56% conversion at −10 °C) and regioregularity (97% HT insertion) to be 3-(*tert*-butyldimethylsiloxy)cyclopentene which has never before been explored or reported. Due to this study, this monomer has now been identified as the ideal choice for isotactic polypentenamer studies moving forward.

1. Introduction

Ring opening metathesis polymerization (ROMP) of low ring strain monomers, such as cyclopentene (CP), is an increasing area of interest due to the large variety of unexplored precision and functionalized elastomeric materials possible [1]. For example, polypentenamers have recently shown promise as recyclable rubber additives [2], styrenic rubbers [3,4], dynamic covalent networks [5], precision polyelectrolytes [6], bottlebrush elastomers [7], and stimuli-responsive materials [8]. The challenges associated with successful ROMP of these monomers involves leveraging the thermodynamics that encapsulate both the enthalpic driving force for polymerization ($-\Delta H_p$), i.e. release of ring strain, and the penalty associated with loss of translational entropy during molecular aggregation ($-\Delta S_p$) [9,10]. Both terms become considerably more complex for low ring strain ROMP when the exergonic free energy ($-\Delta G_p$) is small [1,11,12]. Consequently, the conversion of monomer to polymer becomes highly sensitized to factors that contribute to the Gibbs free energy expression for equilibrium polymerization, such as temperature (T) and monomer concentration [M] [13], as quantified in Eq. (1) [14]. The ΔS_p also becomes particularly interesting since the process of ring opening increases rotational entropy which counteracts some of the loss of translational entropy of polymerization [1,9].

$$\Delta G_p = \Delta H_p - T\Delta S_p = RTln[M] \quad (1)$$

Another factor that warrants considerable attention for ROMP of low strain rings is the size and chemistry of substituents and their effects on thermodynamics. While a majority of ROMP studies have been focused on achiral CP monomers featuring a homoallylic substituent [2,4,5,11,12,15–18], allylic substituted CP monomers are significantly understudied [11,19,20,27]. One major advantage of allylic substituted CPs is that they are chiral and offer the potential to achieve an isotactic branch spaced at every fifth carbon along the backbone [1]. To achieve this, these monomers must be polymerized with regioregular head-to-tail (HT) insertion into the metal alkylidene of metathesis catalysts or else scrambling of the stereochemistry will occur upon head-to-head (HH) and tail-to-tail (TT) propagation. Sita showed that 3-methylcyclopentene undergoes ROMP in a highly regioregular fashion using Schrock-type Mo catalyst [19]. Kobayashi et al. reported a series of allylic substituted *cis*-cyclooctene monomers that propagate in a highly HT regioregular and *trans* fashion with G2 catalyst [21]. This microstructural precision operates through the steric hindrance provided by the allylic substituent; it governs the direction of cycloalkene insertion on the Ru-alkylidene from a distal approach [21–24]. Density function theory (DFT) calculations were also reported by Martinez et al. to further illustrate the mechanistic details and governing factors of this process [25]. Inspired by these reports, our group recently showed that bulky allylic substituted cyclopentene monomers are also able to propagate in a highly regioregular and *trans* fashion with HG2 catalyst to

* Corresponding authors.
E-mail address: jkennemur@fsu.edu (J.G. Kennemur).

https://doi.org/10.1016/j.eurpolymj.2019.109251
Received 21 August 2019; Received in revised form 10 September 2019; Accepted 11 September 2019
Available online 12 September 2019
0014-3057/

produce isotactic polypentenamers from enantiopure monomers [20]. The effects of a precise, 5-carbon isotactic branch periodicity on material properties is particularly intriguing as very few examples of isotactic polyolefins exist outside the more common 2-carbon branch topology [26].

To further develop these isotactic technologies, understanding of the interplay between regioregular insertion and ring strain needs further exploration. Such is the purpose of this study. While the interchange between bulky substituents and regioregular insertion appears effective for CP monomers, allylic substituents often present difficulties with the thermodynamics of ROMP due to reduced ring strain and potential bond order effects on the olefin. Density functional theory studies recently performed on a variety of homoallylic and allylic substituted CPs suggest a mixed variety of ring strains are possible depending on the substituents [15]. However, experimental ROMP on allylic substituted CPs have shown that many have low conversions, if any. [11,19,20]. To the best of our knowledge, these isodesmic equations produce enthalpic quantities (ΔH_p) and may not encapsulate the complex entropic contributions of these polymerizations. Herein, we expand the experimental knowledge of the effect of bulky trialkylsiloxy substitutents on CP and investigate the "give and take" of bulky allylic substituents on ROMP thermodynamics and microstructural regioregularity.

2. Materials and methods

2.1. Materials

Diisobutylaluminum hydride (DIBAL) solution (1.0 M in dichloromethane (DCM)), chlorotriethylsilane (99%), chlorotriisopropylsilane (97%), and toluene-d_8 were purchased from Sigma-Aldich and used as received. 2-Cyclopenten-1-one (99%) and *tert*-butyldimethylchlorosilane were purchased from Oakwood chemicals and used as recieved. Basic alumina and imidazole (99%) were purchased from Beantown Chemicals and used as received. Magnesium sulfate was purchased from EMD Millipore and used as received. Chlorotrimethylsilane was purchased from Fluka Chemicals and used as received. Ethyl vinyl ether (EVE) was purchased from Alfa Aesar and used as received. Hoveyda-Grubbs 2nd generation catalyst (HG2) was donated from Umicore and used as received. Chloroform-*d* was purchased from Cambridge Isotope Laboratories Inc. Anhydrous DCM and toluene were obtained from an SG Waters glass contour solvent purification system under nitrogen that was packed with neutral alumina and the solvents were passed through a 2 μm filter prior to being dispensed.

2.2. Characterizations

^{1}H and ^{13}C NMR experiments were taken on a Bruker Advance III 400 MHz and 600 MHz spectrometer, respectively, unless noted otherwise. Variable Temperature (VT) NMR experiments were taken on a Bruker Advance III 500 MHz spectrometer. Polymers were characterized on an Agilent–Wyatt combination triple detection size exclusion chromatography (SEC) instrument containing 3 successive Agilent PL gel Mixed-C columns (THF mobile phase), and an Agilent 1260 infinity series pump, degasser, autosampler, and thermostatted column chamber. The Wyatt triple detection unit hosts a mini-Dawn TREOS 3-angle light scattering detector, Optilab TrEX refractive index detector, and a Viscostar II differential viscometer. Molar mass and dispersities were determined by a 10-point conventional column calibration with narrow dispersity polystyrene standards varying from 2 to 1800 kDa. Gas chromatography with electron ionization mass spectrometry (GC-EI/MS) was performed at the University of Florida Chemistry Department Mass Spectrometry Research and Education Center. 5 μL of sample was diluted in 1 mL of chloroform prior to analysis. Differential Scanning Calorimetry (DSC) experiments were performed from on a TA Instruments Model Q100 using a heating rate of 10 °C min^{-1} under N_2 flow (40 mL min^{-1}) followed by a cooling rate of 10 °C min^{-1} using an RCS cooler (Model RCS90, refrigerated cooling system). Thermogravimetric analysis (TGA) was performed on a TA Instruments TGA-550 instrument under argon flow (50 mL min^{-1}). Samples were heated to 100 °C, held isothermally for 5 min, and then heated to 550 °C at a rate of 10 °C min^{-1}. Monomer densities (ρ) were determined by gravimetric analysis of a volumetric pycnometer at 23 ± 1 °C. IR spectra were taken on a Perkin Elmer Spectrum 100 Fourier Transform-Infrared (FT-IR) Spectrometer with a ZnSE crystal overcoated with a diamond attenuated total reflectance (ATR) sample chamber.

2.3. Synthesis of cyclopent-2-ene-1-ol (2CPOH).

To a 500 mL flame dried round bottom flask (RBF) equipped with a polytetrafluoroethylene (PTFE)-coated stir bar, 9.00 g (110 mmol) of 2-cyclopenten-1-one and 150 mL of anhydrous DCM was added. The solution was purged with argon for 15 min then cooled to 0 °C. Over 45 min, 150 mL of DIBAL solution (1 M in DCM) was added in 50 mL portions. The solution was then warmed to 23 °C and stirred for 5 h. The reaction was diluted with 100 mL of DCM, cooled to 0 °C, and quenched with 130 mL of a 10:3 v/v water:methanol solution that was added slowly over 30 min. The quenched solution was allowed to stir for 12 h followed by filtering and washing of the filtrate twice with 200 mL of distilled water. The organic phase was collected, dried over $MgSO_4$, and concentrated via rotary evaporation. The crude product was purified by reduced vacuum distillation at 60 °C, 3 torr, affording 4.65 g (55.3 mmol, 49.9% yield) of **2CPOH** as a clear, colorless oil. The product was confirmed by NMR analysis in comparison to previous literature (Figs. S1 and S2) [20].

^{1}H NMR (400 MHz, $CDCl_3$), ppm: 6.00 (m, 1H), 5.84 (m, 1H), 4.86 (s, 1H), 2.52 (m, 1H), 2.26 (m, 2H), 1.70 (m, 2H). ^{13}C NMR (150 MHz, $CDCl_3$), ppm: 135.1. 133.3, 77.58, 33.31, 30.96.

2.4. Synthesis of 3-(trimethylsiloxy)-cyclopentene (M1).

To a 500 mL dry RBF equipped with a PTFE stir bar, 2.00 g (23.8 mmol) of 2CPOH and 150 mL of anhydrous DCM was added and sparged with argon for 15 min. Imidazole (6.48 g, 95.2 mmol) was added and the solution was cooled to 0 °C. Over the course of 15 min, 3.02 mL (23.8 mmol) of chlorotrimethylsilane was added. The solution was gradually warmed to 23 °C then heated to reflux for 14 h. After cooling to room temperature, the precipitated imidazolium salts were filtered and the filtrate was collected and washed twice with 50 mL of distilled water. The organic phase was collected, dried over $MgSO_4$, and then concentrated via rotary evaporation. The crude product was purified by column chromatography with a 95:5 hexane: DCM mobile phase. After solvent removal, 0.8 g (5.1 mmol, 21.6% yield) of pure product was afforded as a clear, colorless oil. The product was confirmed by NMR analysis in comparison to previous literature (Figs. S3 and S4) [20].

^{1}H NMR (400 MHz, $CDCl_3$), ppm: 5.95 (m, 1H), 5.74 (m, 1H), 4.9 (M, 1H), 2.51 (m, 1H), 2.22 (m, 2H), 1.70 (m, 1H), 0.16 (9H). ^{13}C NMR (150 MHz, $CDCl_3$), ppm: 133.93, 133.58, 77.63, 33.33, 31.01, 0.22. ρ (23 ± 1 °C) = 0.856 g cm^{-3}.

2.5. Synthesis of 3-(triethylsiloxy)-cyclopentene (M2).

The same procedure for synthesis and purification of **M1** was performed to produce **M2** with the following exceptions. Chlorotriethylsilane (3.99 mL, 23.8 mmol) was reacted with 2.00 g (23.8 mmol) of 2CPOH. The reaction yielded 2.86 g (14.4 mmol, 60.5% yield) as a clear, colorless oil. The product was confirmed by NMR analysis in comparison to previous literature (Figs. S12 and S13) [20].

^{1}H NMR (400 MHz, $CDCl_3$), ppm: 5.92 (m, 1H), 5.74 (m, 1H), 4.93 (m, 1H), 2.51 (m, 1H), 2.21 (m, 2H), 1.70 (m, 1H), 0.99 (t, 9H), 0.65 (q,

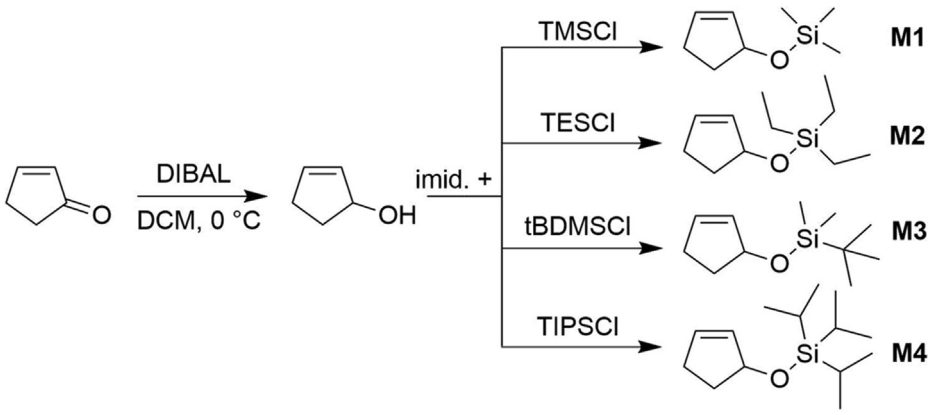

Scheme 1. Synthesis of various allylic-substituted trialkylsiloxy-cyclopentene monomers used in this study.

6). ^{13}C NMR (150 MHz, $CDCl_3$), ppm: 133.80, 133.7, 77.67, 33.53, 31.02, 6.69, 4.86. ρ (23 ± 1 °C) = 0.895 g cm^{-3}.

2.6. Synthesis of 3-(tert-butyldimethylsiloxy)-cyclopentene (M3).

The same procedure for synthesis and purification of **M1** was performed to produce **M3** with the following exceptions. *tert*-Butyldimethylchlorosilane (4.72 g, 23.8 mmol), was reacted with 2.00 g (23.8 mmol) of 2CPOH. The reaction yielded 2.91 g (14.7 mmol, 61.6% yield) as a clear, colorless oil. This new monomer was not reported previously and therefore was confirmed by ^{1}H and ^{13}C NMR analysis in addition to GC-MS (Figs. S21–S23).

^{1}H NMR (400 MHz, $CDCl_3$), ppm: 5.91 (m, 1H), 5.74 (m, 1H), 4.93 (m, 1H), 2.50 (m, 1H), 2.21 (m, 2H), 1.68 (m, 1H), 0.92 (s, 9H), 0.1 (s, 6H). ^{13}C NMR (150 MHz, $CDCl_3$): 133.8, 133.5, 78.13, 33.53, 31.01, 26.0, 18.33, −2.95,-4.53. GC-EI/MS (*m/z*): calcd 198.4, found 198.3. ρ (23 ± 1 °C) = 0.860 g cm^{-3}.

2.7. Synthesis of 3-(triisopropylsiloxy)-cyclopentene (M4).

The same procedure for synthesis and purification of **M1** was performed to produce **M4** with the following exceptions. Chlorotriisopropylsilane (5.09 mL, 23.8 mmol) was reacted with 2.00 g (23.8 mmol) of 2CPOH. The reaction yielded 3.40 g (14.1 mmol, 59.5% yield) as a clear, colorless oil. This new monomer was not reported previously and therefore was confirmed by ^{1}H and ^{13}C NMR analysis in addition to GC-MS (Figs. S33–S35).

^{1}H NMR (400 MHz, $CDCl_3$), ppm: 5.91 (m, 1H), 5.79 (m, 1H), 5.01 (m, 1H), 2.51 (m, 1H), 2.25 (m, 2H), 1.72 (m, 1H), 1.10 (m, 21H). ^{13}C NMR (150 MHz, $CDCl_3$), ppm: 134.13, 133.32, 78.00, 33.91, 31.02, 18.03,12,23. GC-EI/MS (*m/z*): calcd 240.4 found 240.3. ρ (23 ± 1 °C) = 0.887 g cm^{-3}.

2.8. Variable temperature ^{1}H NMR analysis

As a representative example, 0.20 g (1.05 mmol, 0.242 mL) of argon-purged **M3** was added to an NMR tube capped with a septum. In a dry 4 mL vial, 0.171 mL of argon-purged toluene-d_8 was added to 0.6 mg (1.1 μmol, 0.1 mol%) of HG2 catalyst under argon. The catalyst solution was injected into the NMR tube and allowed to react for 3 h at 25 °C. The NMR tube was then placed into the NMR spectrometer at 25 °C and scans were taken to ensure monomer:polymer equilibrium had been established. The NMR sample was then reduced in temperature by 5 °C increments within the spectrometer and scans were taken until equilibrium was established at each temperature. This process was repeated down to 10 °C which is the minimum stable temperature setting for the instrument.

2.9. General polymerization procedure

As a representative example, 0.10 g (0.504 mmol, 0.116 mL) of **M3** was added to a dry 4 mL vial, capped with a rubber septum and purged with argon. Into a separate dry 4 mL vial, 0.6 mg (1.01 μmol, 0.2 mol%) of HG2 was added. The vial was sealed with a rubber septum and purged with argon. Anhydrous and argon-purged toluene (50 μL) was added into the catalyst vial. The catalyst solution was added to the monomer ($[M]_0$ = 3.0 M) and the polymerization was allowed to stir at –10 °C for 5 h. The polymerization was terminated with 0.05 mL of EVE and allowed to stir for 12 h at –10 °C to ensure full termination prior to warming the polymer solution. A crude aliquot was then taken to determine % monomer conversion by ^{1}H NMR (Fig. S28). The remaining solution was warmed to room temperature, diluted with DCM, and passed through a basic alumina column twice. The polymer solution was concentrated slightly via rotary evaporation and precipitated in MeOH. Dissolution and precipitation were done twice. The wet polymer was dried under high vacuum for 12 h. This afforded 0.049 g (89.1% recovery based off of a 56% conversion) of **P3** as a colorless, gummy solid.

3. Results and discussion

To understand the effects of allylic substituents on both the ROMP thermodynamics and the regioselectivity of monomer insertion, four monomers were synthesized through protection of 2CPOH with various trialkylsilyl groups (Scheme 1). The resulting CP monomers, **M1 – M4**, represent a diversified quantity of steric bulk on the allylic position. We reported preliminary evidence that **M2** results in better regioregularity outcomes versus **M1** [20], however, extending the suite of silyl protected monomers to **M3** and **M4** (which are both derived from readily available trialkylchlorosilane precursors) will allow a more complete elucidation of the governing impacts of these monomers with ROMP. Furthermore, from these studies a “Goldilocks” monomer can be determined that marries together the best option for both ROMP thermodynamics and regioregular insertion. NMR spectroscopy within the supporting information confirms the successful synthesis and purification of **M1** and **M2** in addition to new monomers **M3** and **M4** which are also confirmed by high resolution mass spectrometry (HRMS). Densities for all monomers at 23 ± 1 °C were also determined through the gravimetric analysis of a volumetric pycnometer (Table 1).

3.1. Determination of thermodynamic values

The relationship between equilibrium monomer concentration, $[M]_{eq}$ and T is provided in Eq. (2) through rearrangement of Eq. (1). VT ^{1}H NMR allows the determination of $[M]_{eq}$ as a function of T through comparative integration of the unique proton signals associated with

Table 1
Thermodynamic and characterization data of monomer/polymer systems.

ID	Monomer specifics					Polymer specifics					
	$\rho_{23\,°C}$ (g cm^{-3}) [a]	$[M]_{bulk}$ (mol L^{-1})	$-\Delta H_p$ (kJ mol^{-1})[b]	$-\Delta S_p$ (J mol^{-1} K^{-1})[b]	$T_{c,\,bulk}$ (°C)	M_n (kg mol^{-1})[c]	Đ[c]	HT (%)[d]	*trans* (%)[e]	T_g (°C)[f]	T_d (°C)[g]
M1/P1	0.856	5.47	12.66	49.95	80	173.6	1.68	80.3	95.7	< −60	275
M2/P2	0.895	4.51	21.26	80.20	41	121.3	1.51	89.5	96.0	−50	273
M3/P3	0.860	4.33	6.84	29.59	120	296.4	1.52	96.7	94.6	−4	265
M4/P4	0.887	3.69	n.d.	n.d.	n.d.	91.3	1.44	> 99	95.5	−11	340

[a] Determined by pycnometry at 23 ± 1 °C.
[b] Determined by VT-^{1}H NMR.
[c] Determined by SEC versus polystyrene standards.
[d] Determined by ^{1}H NMR using deconvolution of peaks analysis.
[e] Determined by ^{1}H NMR using deconvolution of peaks analysis.
[f] Determined by DSC.
[g] Determined by TGA analysis at the point of 5% mass loss.

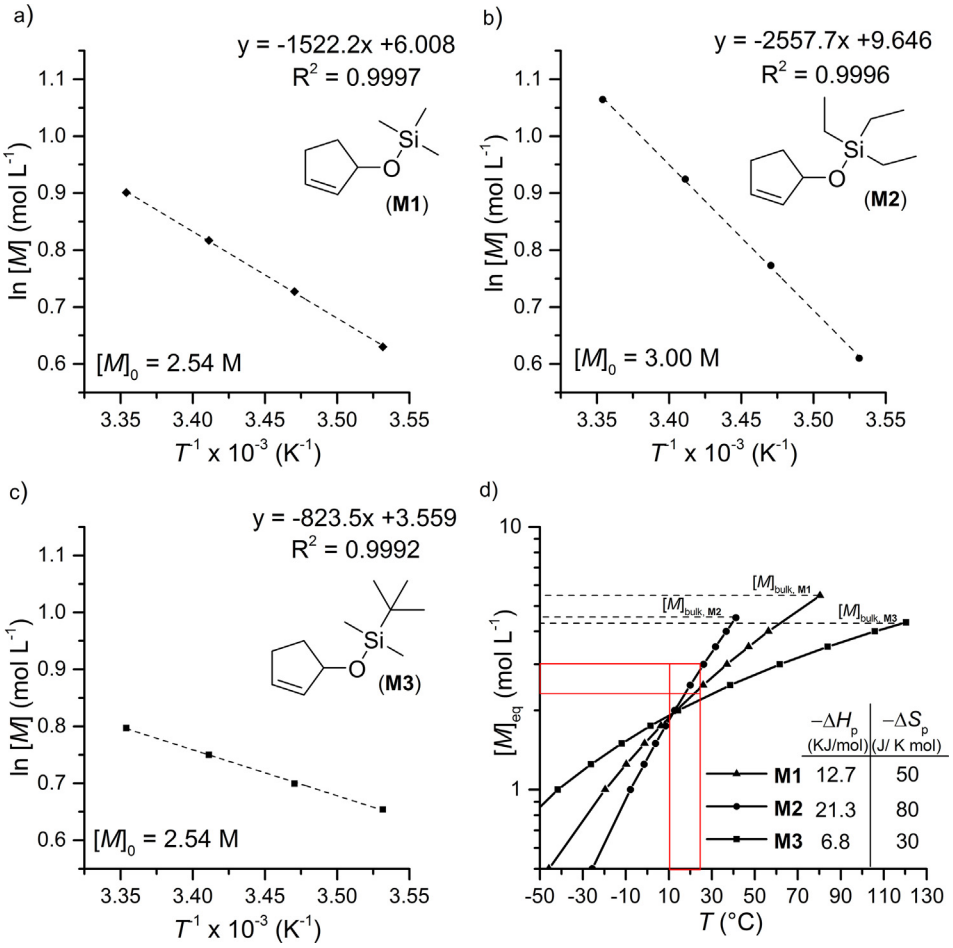

Fig. 1. Logarithmic equilibrium monomer concentration as a function of inverse temperature (between 10 and 25 °C) for (a) **M1** ($[M]_0$ = 2.54 M), (b) **M2** ($[M]_0$ = 3.00 M), and (c) **M3** ($[M]_0$ = 2.54 M) as determined by variable temperature ^{1}H NMR analysis using integration ratio comparison between the monomer and polymer olefin proton peaks. Each experiment was performed in toluene-d_8 using HG2 catalyst at 0.1 mol% of monomer. The linear regression equations provided were used to determine ΔH_p and ΔS_p. (d) Equilibrium monomer concentration as a function of temperature for **M1** (triangles), **M2** (circles), and **M3** (squares). Solid line traces represent the ceiling temperature (T_c) for each monomer based on concentration as determined by the ΔH_p and ΔS_p values provided by data in (a-c). Horizontal dashed lines represent the bulk monomer concentration of each monomer. The solid red box columns outline the temperature and concentration range where ΔH_p and ΔS_p were determined. (For interpretation of the references to colour in this figure legend, the reader is referred to the web version of this article.)

monomer and polymer olefin signals (Figs. S7, S16, S27, S39) at a specific T. Once equilibrium is established (i.e. the integration ratios no longer change) $[M]_e$ can be calculated for that T and the process is repeated at a new T. This design of experiments was performed on **M1 – M4** in toluene-d_8 using HG2 catalyst at a 0.1 mol% ratio compared to the initial moles of monomer. Equilibrium was monitored between 10 and 25 °C at 5 °C intervals starting from known initial monomer concentrations, $[M]_0$, between 2.54 and 3.00 M. Logarithmic $[M]_e$ as a function of inverse T is plotted for **M1**, **M2**, and **M3** in Fig. 1 a-c, respectively. A linear regression analysis of this data allows determination of ΔH_p and ΔS_p in accordance with Eq. (2) which are provided in Table 1. **M4**, predicted to be the bulkiest monomer of the set, displayed no conversion to polymer at even the coldest temperature (10 °C).

$$\ln[M]_{eq} = \frac{\Delta H_p}{RT} - \frac{\Delta S_p}{R} \quad (2)$$

Monomer ring strain ($-\Delta H_p$) is often the parameter of focus for the efficacy of ROMP and a survey of these values in Table 1 shows that **M2** (21.3 kJ mol^{-1}) is significantly higher than **M1** (12.7 kJ mol^{-1}) and **M3** (6.8 kJ mol^{-1}). By using ΔH_p alone, it would be concluded that **M2** is the most thermodynamically favorable monomer regardless of T. However, when also factoring in experimentally determined ($-\Delta S_p$) to the calculation of critical monomer concentrations at varying temperatures, as shown in Fig. 1d, it becomes apparent that $-\Delta H_p$ alone does not fully encapsulate the thermodynamics. In fact, the extrapolated ceiling temperature of bulk monomer $T_{c,bulk}$ of **M3** (horizontal dashed lines in Fig. 1d) is 120 °C, which is ~80 °C higher than $T_{c,bulk}$ of

M2 (Table 1). This phenomenon draws directly from the differences in $-\Delta S_p$ between **M2** (80 J mol^{-1} K^{-1}) and **M3** (30 J mol^{-1} K^{-1}). In other words, the entropic penalty for ROMP of **M3** appears significantly reduced. Although the exact reasoning warrants further investigation, it may be hypothesized from the varying degrees of rotational entropy that are gained in the ring-opened state by each specific monomer; each serves to reduce the translational entropic penalty to varying degrees. **M1** exhibited an intermediate $-\Delta S_p$ (50 J mol^{-1} K^{-1}) when compared to **M2** and **M3** (Table 1).

Fig. 1d also provides a rational design blueprint for anticipated monomer conversion of ROMP performed at various temperatures. The solid line traces represent the lower limit of $[M]_{eq}$. Any conditions of $[M]$ and T below and to the right of these lines would not be expected to produce polymer. Any conditions above/left of the lines (with an upper limit of the dashed lines, $[M]_{bulk}$) would produce polymer until the solid lines, $[M]_{eq}$, are reached. To test this, ROMP of **M3** was performed at −10 °C with $[M]_0$ = 3.00 M (see experimental). The resulting % monomer conversion after was 56% (Fig. S28), which is close to the theoretical value (49%) predicted from Fig. 1d.

3.2. Determination of regioregularity outcomes

The combination of ^{1}H and ^{13}C NMR allows direct insight into the microstructural regularity of the polymers produced. Specifically, methine proton signals resulting from HT and HH regioisomers produce unique shifts in ^{1}H NMR that allow peak deconvolution analysis and quantification of %HT and %*trans* content of the materials. Polymers (**P1 – P3**) were produced from monomers (**M1 – M3**), respectively, at cold temperature (−10 °C) and $[M]_0$ = 3.0 M. At these conditions, **M4**, still did not produce polymer. Therefore we performed a final ROMP of **M4** in bulk (3.69 M) at −10 °C and found that ~14% monomer conversion ($[M]_{eq}$ = 3.2 M at −10 °C) was achieved under these conditions (Figure S40), providing enough polymer for analysis. It is clear, however, that **M4** has the least favorable thermodynamics for ROMP. Fig. 2 displays the ^{1}H NMR analysis of **P1 – P4** in $CDCl_3$. While the full spectrum with annotated peaks are provided at the bottom of each figure quadrant, the insets display zoomed in regions of interest for microstructure determination. The olefin signal region between 5.2 and 5.8 ppm (blue dashed box) shows unique signals associated with the *trans*-head-to-tail (*t*-HT) and *cis*-head-to-tail isomers in addition to the expected splitting (doublet-of-doublets at ~5.40 ppm and doublet-of-triplets at ~5.55 ppm) of the major *t*-HT signals for each polymer. More importantly, the methine proton region between 3.75 and 4.50 ppm (red solid boxes) display unique signals for both the *t*-HT (4.05–4.11 ppm) and the *trans*-head-to-head (*t*-HH) protons (4.96–4.05 ppm) in addition to the (*c*-HT) signal. Although the *t*-HH and *t*-HT are not fully resolved, a deconvolution of peak analysis allows the approximate determination of the % HT content within the microstructure (Figs. S45 – S48) in addition to the overall % *trans* content. These values are provided for **P1**-**P4** in Table 1. While each polymer contains approximately the same amount of *trans* isomers (95 ± 1%), the regioregularity outcomes are highly influenced by the sterics of each monomer substituent. **P1** and **P2** contain HT regioregularity of 80.3 and 89.5% which is slightly improved for **P1 (**68%) and nearly the same for **P2** (92%) as our previous report [20]. However, **P3** and **P4** resulted in superior regioregularity of 96.7 and > 99% HT, respectively.

The high degree of microstructural regularity displayed by these systems can also be seen in ^{13}C NMR analysis (Fig. 3). The presence of additional olefin carbon signals (dashed blue boxes, 129–135 ppm) and methine signals (solid red boxes, 70–76 ppm), in addition to their relative size, is a qualitative display of their regioirregularity. While these signals are seen for **P1** and **P2**, they are completely absent for highly regioregular **P3** and **P4** within the limits of the signal-to-noise ratio.

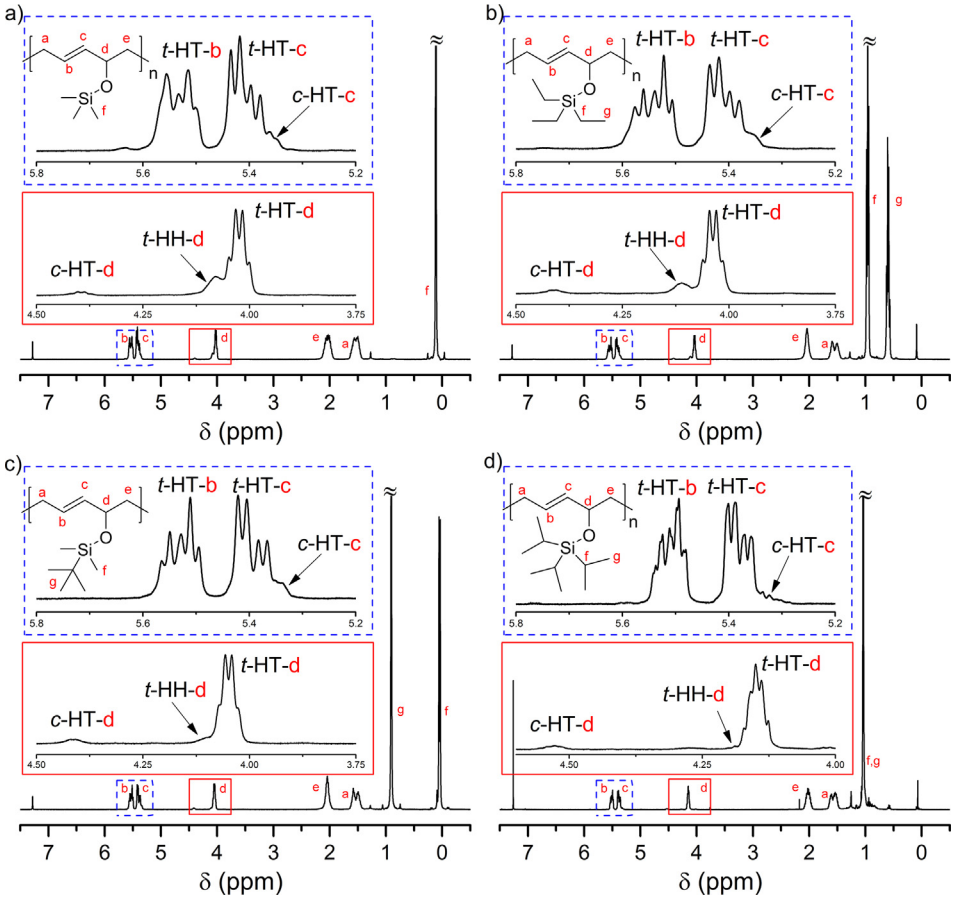

Fig. 2. ^{1}H NMR spectra ($CDCl_3$, 25 °C) of (a) **P1**, (b) **P2**, (c) **P3**, and (d) **P4** with chemical structures and peaks annotated. The dashed line (blue) boxes surround the olefin proton region which is amplified in the top inset of each plot. The solid line (red) boxes surround the backbone methine proton which is amplified in the bottom inset of each plot. Peaks associated with *trans* regioregular head-tail (*t*-HT), *cis* regioregular head-tail (*c*-HT), and *trans* head-head isomers (*t*-HH) signals are annotated in each inset for the corresponding proton peaks. (For interpretation of the references to colour in this figure legend, the reader is referred to the web version of this article.)

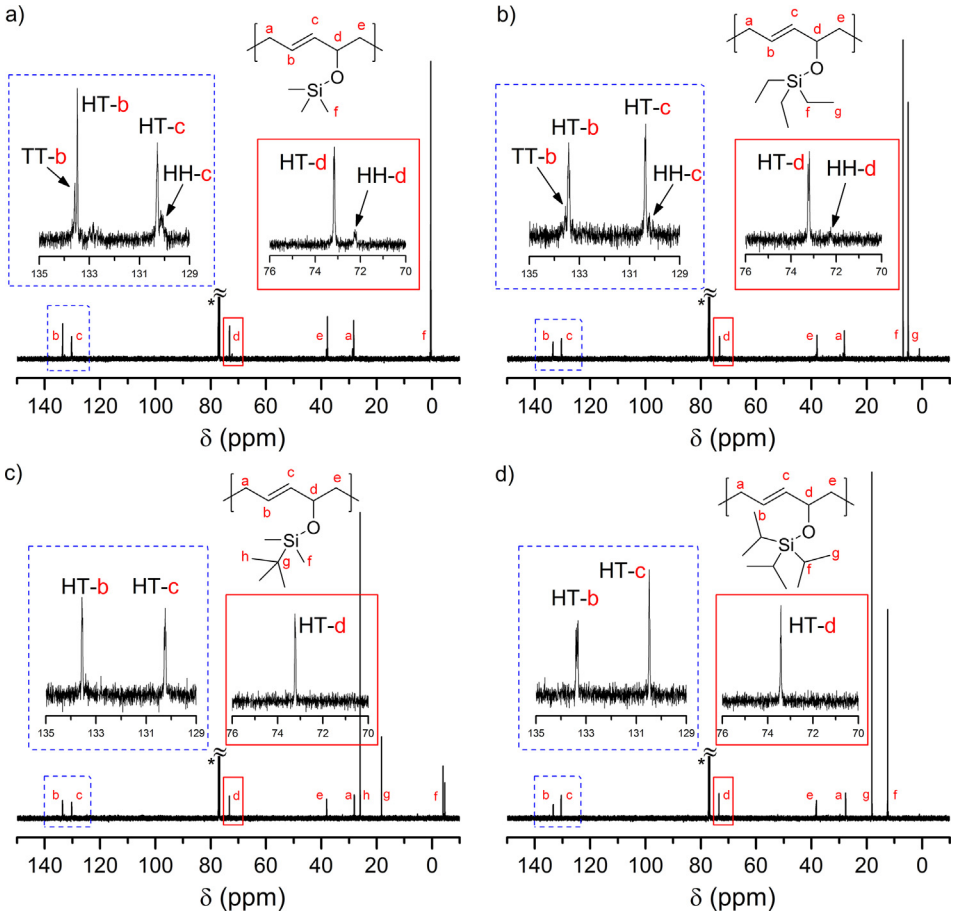

Fig. 3. ^{13}C NMR spectra ($CDCl_3$, 25 °C) of (a) **P1**, (b) **P2**, (c) **P3**, and (d) **P4** with chemical structures and peaks annotated. The dashed line (blue) boxes surround the olefin carbon region which is amplified in the left inset of each plot. The solid line (red) boxes surround the backbone methine carbon which is amplified in the right inset of each plot. Regioregular head-tail (HT) isomer signals are only seen in **P3** and **P4** while some head-head (HH) and tail-tail (TT) isomer signals are seen in **P1** and **P2**. (For interpretation of the references to colour in this figure legend, the reader is referred to the web version of this article.)

Hence, ^{13}C NMR analysis is an effective method to qualitatively confirm the regioregular outcomes concluded by ^{1}H NMR analysis.

3.3. Other polymer characterizations

Size exclusion chromatography of each polymer in THF reveals substantial molar masses (100 – 300 kg mol^{-1}) and moderate dispersities, Đ, between 1.4 and 1.7 (Table 1). Based on the 500:1 monomer to catalyst ratios used, the resulting molar masses are much higher than theoretical and suggest that initiation at −10 °C is much slower than propagation. This outcomes agrees with similar cold initiation problems displayed by Ru-based catalysts discussed in our previous ROMP studies.[4, 13] It is possible that a variable temperature ROMP[13] may improve upon these outcomes, however, neither targeted molar mass or narrow Đ are necessary for the purposes of this study. The high molar masses do allow for accurate analysis of the glass transition temperatures (T_g) of these polymers. DSC reveals an interesting range of T_g values that result from the different trialkylsiloxy pendants on the polypentenamers (Figs. S11, S20, S32, S44). While **P1** and **P2** exhibit low T_g (≤ −50 °C), consistent with previous literature [20], **P3** and **P4** display greatly increased values of −4 and −11 °C, respectively (Table 1). These outcomes suggest that bulky allylic substituent not only modulate the regioregularity and ROMP thermodynamics, but also the thermal properties of the resulting materials. TGA analysis of the thermal decomposition temperature (T_d), taken at the point of 5% mass loss, reveals a good thermal stability for these systems (Table 1). While T_d for **P1**, **P2**, and **P3**, were between 265 and 275 °C, **P4** had a much higher value of 340 °C. The reason for this enhanced thermal stability may possibly be attributed to the relative stability of the triisopropylsiloxy (TIPS) group but may also be effected by the extremely regioregular microstructure of **P4** which has very few olefins that contain the TIPS group on both sides of the olefin from a HH regioisomer.

4. Conclusions

An in-depth study on the thermodynamics and microstructural outcomes from ROMP of four different allylic trialkylsiloxy-substituted cyclopentene monomers has been investigated. The order of calculated $[M]_{eq}$ (mol L^{-1}) at −10 °C was determined to be **M2** (0.93) < **M1** (1.25) < **M3** (1.53) ≪ **M4** (~3.2). However, due to slight differences in $[M]_{bulk}$ and significant differences in experimentally determined ΔS_p at similar concentrations, the bulk T_c values follow a nearly opposite trend (**M3** (120 °C) > **M1** (80 °C) > **M2** (41 °C). These outcomes suggest that the complete thermodynamics with ΔS_p and not just ring strain ΔH_p are important parameters that govern the successful ROMP of low strain cyclopentenes at varying T. While all polymers produced had a %*trans* olefin content of 95 ± 1%, the steric bulk of the substituent had a great effect on the regioregularity. **P1** had the lowest % HT (~80%) while **P4** had a near perfect regioregular structure (> 99% HT). However, **M4** was by far the worst monomer from a thermodynamics approach and only reached 14% monomer conversion from bulk at −10 °C. The regioregularity of **P3** (~97% HT) was significantly higher than **P2** (~90% HT). Interestingly, the T_g value of **P3** (−4 °C) was also significantly higher than **P2** (−50 °C). Therefore our search for a "Goldilocks" monomer that produces both adequate thermodynamics and superior levels of microstructural regularity concludes with the discovery of a new monomer/polymer system, **M3**/**P3**, which satisfies this criterion for future isotactic polypentenamer studies.

Declaration of Competing Interest

None.

Acknowledgements

This work was supported by the National Science Foundation under Grant No. 1750852. We thank Umicore for generous donation of Ru catalyst M72 (HG2). ^{1}H and ^{13}C NMR were performed in the FSU Department of Chemistry and Biochemistry NMR Facility under supervision of Dr. Banghao Chen. Mass spectrometry was provided by the UF Mass Spectrometry and Education Center funded under NIH S10 OD021758-01A1.

Data availability

The raw data required to reproduce these findings can be obtained upon request to jkennemur@fsu.edu.

Appendix A. Supplementary material

Supplementary data to this article can be found online at https://doi.org/10.1016/j.eurpolymj.2019.109251.

References

[1] W.J. Neary, J.G. Kennemur, Polypentenamer Renaissance: Challenges and Opportunities, ACS Macro Lett. 8 (2019) 46–56.
[2] R. Tuba, J. Balogh, A. Hlil, M. Barłóg, M. Al-Hashimi, H.S. Bazzi, Synthesis of recyclable tire additives via equilibrium ring-opening metathesis polymerization, ACS Sustain. Chem. Eng. 4 (2016) 6090–6094.
[3] R.J. Kieber, W.J. Neary, J.G. Kennemur, Viscoelastic, mechanical, and glasstomeric properties of precision polyolefins containing a phenyl branch at every five carbons, Ind. Eng. Chem. Res. 57 (2018) 4916–4922.
[4] W.J. Neary, J.G. Kennemur, A precision ethylene-styrene copolymer with high styrene content from ring-opening metathesis polymerization of 4-phenylcyclopentene, Macromol. Rapid Commun. 37 (2016) 975–979.
[5] H. Liu, A.Z. Nelson, Y. Ren, K. Yang, R.H. Ewoldt, J.S. Moore, Dynamic remodeling of covalent networks via ring-opening metathesis polymerization, ACS Macro Lett. 7 (2018) 933–937.
[6] A. Kendrick, W.J. Neary, J.D. Delgado, M. Bohlmann, J.G. Kennemur, Precision polyelectrolytes with phenylsulfonic acid branches at every five carbons, Macromol. Rapid Commun. 39 (2018) 1800145.
[7] W.J. Neary, B.A. Fultz, J.G. Kennemur, Well-defined and precision-grafted bottlebrush polypentenamers from variable temperature ROMP and ATRP, ACS Macro Lett. (2018) 1080–1086.
[8] W.J. Neary, T.A. Isais, J.G. Kennemur, Depolymerization of polypentenamer bottlebrushes and their Macromolecular Metamorphosis, J. Am. Chem. Soc. 141 (2019) 14220–14229.
[9] K.J. Ivin, Thermodynamics of addition polymerization, J. Polym. Sci., Part A: Polym. Chem. 38 (2000) 2137–2146.
[10] K.J. Ivin, J.C. Mol, Olefin Metathesis and Metathesis Polymerization, Academic Press, San Diego, CA, 1997.
[11] A. Hejl, O.A. Scherman, R.H. Grubbs, Ring-opening metathesis polymerization of functionalized low-strain monomers with ruthenium-based catalysts, Macromolecules 38 (2005) 7214–7218.
[12] A.R. Hlil, J. Balogh, S. Moncho, H.-L. Su, R. Tuba, E.N. Brothers, M. Al-Hashimi, H.S. Bazzi, Ring opening metathesis polymerization (ROMP) of five- to eight-membered cyclic olefins: computational, thermodynamic, and experimental approach, J. Polym. Sci. Part A: Polym. Chem. 55 (2017) 3137–3145.
[13] W.J. Neary, J.G. Kennemur, Variable temperature ROMP: leveraging low ring strain thermodynamics to achieve well-defined polypentenamers, Macromolecules 50 (2017) 4935–4941.
[14] P.C. Hiemenz, T. Lodge, Polymer Chemistry, 2nd ed., CRC Press, Boca Raton, 2007.
[15] R. Tuba, M. Al-Hashimi, H.S. Bazzi, R.H. Grubbs, One-pot synthesis of poly(vinyl alcohol) (PVA) copolymers via ruthenium catalyzed equilibrium ring-opening metathesis polymerization of hydroxyl functionalized cyclopentene, Macromolecules 47 (2014) 8190–8195.
[16] S. Song, Z. Zhang, X. Liu, Z. Fu, J. Xu, Z. Fan, Synthesis and characterization of functional polyethylene with regularly distributed thioester pendants via ring-opening metathesis polymerization, J. Polym. Sci. Part A: Polym. Chem. 55 (2017) 4027–4036.
[17] S. Song, Z. Xing, Z. Cheng, Z. Fu, J. Xu, Z. Fan, Functional polyethylene with regularly distributed ester pendants via ring-opening metathesis polymerization of ester functionalized cyclopentene: synthesis and characterization, Polymer 129 (2017) 135–143.
[18] S. Song, Z. Fu, J. Xu, Z. Fan, Synthesis of functional polyolefins via ring-opening metathesis polymerization of ester-functionalized cyclopentene and its copolymerization with cyclic comonomers, Polym. Chem. 8 (2017) 5924–5933.
[19] L.R. Sita, Main-chain chiral polymers from β-citronellene via tandem diene metathesis cyclization/ring-opening metathesis polymerization, Macromolecules 28 (1995) 656–657.
[20] S. Brits, W.J. Neary, G. Palui, J.G. Kennemur, A new echelon of precision polypentenamers: highly isotactic branching on every five carbons, Polym. Chem. (2018).
[21] S. Kobayashi, L.M. Pitet, M.A. Hillmyer, Regio- and stereoselective ring-opening metathesis polymerization of 3-substituted cyclooctenes, J. Am. Chem. Soc. 133 (2011) 5794–5797.
[22] S. Kobayashi, K. Fukuda, M. Kataoka, M. Tanaka, Regioselective ring-opening metathesis polymerization of 3-substituted cyclooctenes with ether side chains, Macromolecules 49 (2016) 2493–2501.
[23] H. Martinez, J. Zhang, S. Kobayashi, Y. Xu, L.M. Pitet, M.E. Matta, M.A. Hillmyer, Functionalized regio-regular linear polyethylenes from the ROMP of 3-substituted cyclooctenes, Appl. Petrochem. Res. 5 (2015) 19–25.
[24] K. Osawa, S. Kobayashi, M. Tanaka, Synthesis of sequence-specific polymers with amide side chains via regio-/stereoselective ring-opening metathesis polymerization of 3-substituted cis-cyclooctene, Macromolecules 49 (2016) 8154–8161.
[25] H. Martinez, P. Miró, P. Charbonneau, M.A. Hillmyer, C.J. Cramer, Selectivity in ring-opening metathesis polymerization of Z-cyclooctenes catalyzed by a second-generation grubbs catalyst, ACS Catal. 2 (2012) 2547–2556.
[26] J.H. Zhang, M.E. Matta, H. Martinez, M.A. Hillmyer, Precision Vinyl Acetate/Ethylene (VAE) copolymers by ROMP of acetoxy-substituted cyclic alkenes, Macromolecules 46 (2013) 2535–2543.
[27] K. Song, K. Kim, D. Hong, J. Kim, C.E. Heo, H.I. Kim, S.H. Hong, Highly active ruthenium metathesis catalysts enabling ring-opening metathesis polymerization of cyclopentadiene at low temperatures, Nat. Commun. 10 (2019) 3860, , https://doi.org/10.1038/s41467-019-11806-5 (in press).